Supplementary materials for:

Intensity of repetitive negative thinking in depression is associated to connectivity between semantic processing and emotion regulation areas

Aki Tsuchiyagaito[1-3#], Stella M. Sánchez[1], Masaya Misaki[1], Rayus Kuplicki[1], Heekyong Park[1,4], Martin P. Paulus[1], and Salvador M. Guinjoan[1]

[1]Laureate Institute for Brain Research, Tulsa, OK, USA
[2]The University of Tulsa, Tulsa, OK, USA
[3]Chiba University, Chiba, Japan
[4]University of North Texas at Dallas, Dallas, TX, USA

[#] Corresponding author:
Aki Tsuchiyagaito, email: atsuchiyagaito@laureateinstitute.org

Table of Contents

Supplementary Method

1. Neuroimaging data acquisition and preprocessing

All the participants went through an anatomical scan and then two six-minute resting-state fMRI scans were obtained subsequently, separated by a short break (Cho, Korchmaros, Vogelstein, Milham, & Xu, 2021). During the resting-state fMRI scans, participants were instructed not to think anything in particular, and to be relaxed while looking at a cross on the screen. For the anatomical reference, T1-weighted MRI images with a magnetization-prepared rapid gradient-echo (MPRAGE) sequence were acquired with the following imaging parameters:
FOV = 256 mm, matrix = 256 × 256, slice thickness = 1.0 mm producing 1mm isotropic voxels, 208 sagittal slices, TR/TE = 6/2.92 ms, SENSE acceleration factor R = 2, flip angle = 8°, inversion time TI = 1400/1060 ms, sampling bandwidth = 31.25 kHz, scan time = 6 min 11 s.
For the resting-state fMRI, a single-shot gradient-recalled echo-planner imaging (EPI) sequence with sensitivity encoding (SENSE) was used with the following imaging parameters:
TR/TE = 2000/27 ms, flip angle = 78°, FOV/slice = 240/2.9 mm, 39 axial slices, SENSE acceleration factor R = 2, 96 × 96 matrix reconstructed into 128 × 128 image resulting into 1.875 × 1.875 × 2.9 mm^3 voxels volume, sampling bandwidth = 250 kHz, scan time = 6 min (180 TRs).

2. Anatomical and functional MRI data preprocessing

Imaging data process were performed with SPM12 (Wellcome Department of Imaging Neuroscience, UCL, London, UK), CONN-toolbox (version 20.b) (Whitfield-Gabrieli & Nieto-Castanon, 2012), implemented in Matlab R2019a (The MathWorks Inc., Natick, MA, USA). The initial three volumes were discarded to avoid magnetic saturation effects. To aggregate the fMRI data, we first preprocessed the data and concatenated the preprocessed data for the subsequent analyses (Cho et al., 2021). The default preprocessing pipeline implemented in CONN-toolbox was performed for both anatomical and functional imaging. Those preprocessing pipeline included functional realignment and unwarp, slice-timing and motion correction, outlier detection, segmentation of gray matter (GM), white matter (WM) and cerebrospinal fluid (CSF), normalization to Montreal Neurological Institute (MNI) space, and partial smoothing (6 mm full width at the half maximum Gaussian kernel). During the outlier detection step, acquisitions with framewise displacement (FD) above 0.25 mm or global mean intensity above three standard deviations were flagged/scrubbed as potential outliers using the Artefact Detection Tools (ART: www.nitrc.org/projects/artifact_detect). Ten subjects were removed from the dataset before the propensity score matching procedure since they did not maintain at least 6 minutes of scanning time after the scrubbing (Van Dijk et al., 2010). Additionally, mean FD was used as a covariate of no interest in all second-level analyses. After the preprocessing, denoising of the functional data was performed using a component-based noise correction method, (CompCor) by taking into account five orthogonal time series and their derivatives from WM and CSF(Behzadi, Restom, Liau, & Liu, 2007), linear detrending to remove the linear signal drift, temporal band-pass filtering (0.008-0.09 Hz) to remove physiological, estimated subject-motion parameters (3 rotation and 3 translation parameters and 6 other parameters representing their first order time derivatives), and scrubbing parameters derived from the ART.

3. Multivariate correlation (MCOR) analysis

First, for a single voxel of interest, the functional connectivity between this voxel and the rest of the brain for every subject were calculated. Since we have 100 subjects, 100 'seed'-to-voxel maps were created using our original voxel of interest as 'seed'. We gathered those maps into a M × N matrix, where M is the number of subjects (100 in our study), and N is the number of voxels in the brain. Next, a singular value decomposition (SVD) of this matrix was applied jointly across all subjects, but separately for each seed-to-voxel connectivity map, to obtain a lower-dimensional representation of the original matrix. The choice of number of K principal components was made to capture most of the between subjects' variability in connectivity patterns between our voxel of interest and the rest of the brain. Following prior studies, the first five components were retained as they explained xx% of the between-subjects variance in whole-brain connectivity at each voxel. As a result, a set of K components (a K × N matrix of spatial components) as well as a set of K principal component scores (a K × M matrix of component scores). Then, an F-test of the group difference (High RNT vs. Low RNT) for each component score was performed, and the omnibus statistic across the K tests was mapped onto the seed voxels. This process was repeated for whole-brain voxels as a seed to identify voxels that showed significant differences in functional connectivity patterns between High RNT and Low RNT groups.

4. ROI-to-ROI analysis within the DMN

4.1. Definition of ROIs within the DMN

According to the previous work (Andrews-Hanna, Reidler, Sepulcre, Poulin, & Buckner, 2010) , 11 ROIs of the DMN were defined using 8-mm radius spheres, including the anterior medial prefrontal cortex (aMPFC, MNI [-6, 52, -2]), posterior cingulate cortex (PCC, MNI [-8, -56, 26]), dorsal medial prefrontal cortex (dMPFC, MNI [0, 52, 26]), temporoparietal junction (TPJ, MNI [-54, -54, 28]), lateral temporal cortex (LTC, MNI [-60, -24, -18]), temporal pole (TempP, MNI [-50, 14, -40]), ventral medial prefrontal cortex (vMPFC, MNI [0, 26, -18]), posterior inferior parietal lobule (pIPL, -44,-74,32), retrosplenial cortex (Rsp, MNI [-14, -52, 8]), parahippocampal cortex (PHC, MNI [-28, -40, -12]) and hippocampal formation (HF, MNI [-22, -20, -26]). The aMPFC and PCC constitute the midline core of the DMN. The dMPFC subsystem includes the dMPFC, TPJ, LTC and TempP. The MTL subsystem comprises the vMPFC, pIPL, Rsp, PHC and HF.

4.2. ROI-to-ROI functional connectivity calculations

Functional connectivity analyses were performed based on the 11 ROIs in the DMN with SPM12 (Wellcome Department of Imaging Neuroscience, UCL, London, UK), CONN-toolbox (version 20.b) (Whitfield-Gabrieli & Nieto-Castanon, 2012), implemented in Matlab R2019a (The MathWorks Inc., Natick, MA, USA). The average time series from each ROI were extracted, and Pearson's correlations were calculated between any two nodes of 11 ROIs for each subject. Fisher's r-to-z transformation was applied to normalize the correlation coefficients, and we obtained a 11 × 11 functional connectivity matrix for each subject.

4.3. ROI-to-ROI functional connectivity within the DMN in high RNT and low RNT

To examine group differences in the functional connectivity matrix, analysis of covariance (ANOVA) adjusted for mean head motion was performed on the half of 11 × 11 functional

connectivity (i.e., 55 connectivity) matrices due to the symmetry. The statistical significance level was set at $p < 0.05$ (FDR correction).

4.4. Correlation analysis between ROI-to-ROI functional connectivity within the DMN, and clinical symptoms

To reduce the number of correlation analyses, the average within-system and inter-system connectivity of three DMN subsystems for each subject were calculated. The average within-system connectivity is defined as the mean of the sum of all edges in one subsystem, while the average inter-system functional connectivity is referred to the mean of the sum of functional connectivity strength of all edges between two subsystems. This procedure resulted in three within-system (i.e., midline core, dMPFC subsystem, and MTL subsystem), and three inter-system (i.e., midline core – dMPFC subsystem, midline core – MTL subsystem, and dMPFC subsystem – MTL subsystem). To examine the association between those six within- and inter-subsystem and the level of clinical symptoms, Pearson's correlations were calculated between the z-values of six within- and inter- subsystem connectivity and symptom variables (i.e., HAMD, PHQ, OASIS, and RRS brooding subscale). The statistical significance level was set at $p < 0.05$ (FDR correction).

Supplementary Results

1. ROI-to-ROI functional connectivity within the DMN in high RNT and low RNT

The average 55 functional connectivity matrices are displayed for both high RNT (n=50, Fig. S1A) and low RNT (n=50, Fig. S1B) groups. MDD individuals with high RNT showed similar connectivity patterns among 11 ROIs as those with low RNT. There was no significant difference in connectivity patterns between two groups.

2. Correlation analysis between ROI-to-ROI functional connectivity within the DMN, and clinical symptoms

In MDD participants (n=100), after controlling for mean head motion, we observed positive correlations between midline core and HAMD score, although a positive correlation between midline core and HAMD score did not survive after FDR correction (Fig. S2). We did not find any significant associations related to inter-system connectivity and symptom scores.

Supplementary Discussion

1. Anterior Insular cortex hyperconnectivity with speech-related areas in MDD subjects with high RNT

We also observed that the right STS displays hyperconnectivity with the bilateral AI in individuals with high RNT. The AI (especially on the right hemisphere) is considered as the main node of a hub referred to as *salience network* (SN), which commands transitions between the DMN and *executive control network* (ECN), according to the current emotional salience in relation to the inner and outer relevant stimuli (Menon, 2011; Menon & Uddin, 2010). In this way, AI enables attention shift and task engagement. The insular cortex has been related to disparate cognitive, affective, and regulatory functions, including interoceptive awareness, emotional responses, and empathic processes (Menon & Uddin, 2010). The insular cortex has been proposed as the site the direct mapping of internal bodily and feeling states (Craig, 2002, 2003, 2009). This mapping forms the basis for predictions of physiological reactions to emotional stimuli with respect to the self, shaping subjective and self-related feeling states

(Lamm & Singer, 2010). Similarly, Paulus and Stein (Paulus & Stein, 2010) proposed a critical role of the AI in depression and anxiety, in that both conditions represent altered interoceptive states as a consequence of reduced ability to adequately report interoceptive afferents, and of exaggerated response to aversive interoceptive afferents. By playing a critical role in mediating self-awareness, body integrity, and integrating peripheral autonomic output (Critchley, Melmed, Featherstone, Mathias, & Dolan, 2002; Critchley, Wiens, Rotshtein, Ohman, & Dolan, 2004; Paulus & Stein, 2010) , the AI serves as a strategic neural node in the appraisal of emotional responses (Craig, 2009). According to the response styles theory (Nolen-Hoeksema, 2000), RNT consists of repetitive and passive thoughts about the possible causes and consequences of *negative events*, and is conceptualized as a cognitive pattern of response to *negative affects*. In this context, AI hyperconnectivity with right STS could be a neural mechanism explaining the link between the cognitive and the emotional aspects of RNT. Elevated connectivity between STS and AI in high RNT individuals might thus indicate that RNT is linked to increased sensitivity to salient self-referential information.

Another important aspect of the mental habit view of RNT is that habitual responses to the negative events are evoked "automatically" (i.e., without conscious effort) by contextual cues, which distinguish RNT from other forms of spontaneous thoughts (e.g., daydreaming, mind wandering, and creative thoughts) and deliberately constrained thoughts (e.g., distraction, reappraisal, acceptance, and mindfulness) (Christoff, Irving, Fox, Spreng, & Andrews-Hanna, 2016). A recent meta-analysis studying perseverative cognition (Makovac, Fagioli, Rae, Critchley, & Ottaviani, 2020) reported that, in contrast to the DMN (which normally supports non-pathological self-referential processes, especially mind wandering), the AI plays a crucial role in the regulation of autonomic arousal (Beissner, Meissner, Bar, & Napadow, 2013; Craig, 2002, 2003, 2009; Critchley et al., 2003; Critchley et al., 2004; Thayer, Ahs, Fredrikson, Sollers, & Wager, 2012), and thus possibly contributes to abnormal patterns of cardiovascular, autonomic, and endocrine systems activity characteristic of RNT (Ottaviani et al., 2016). Thus, RNT may relate to the function of AI in detecting and responding to the salient stimuli (Makovac et al., 2020; Tozzi et al., 2021) rather than the DMN-related self-referential thoughts in mPFC and PCC/precuneus (Hamilton, Farmer, Fogelman, & Gotlib, 2015). This automatic response may be enhanced in chronic ruminators and worriers, which leads in turn to difficulties in disengaging attention from salient event detection (Verkuil, Brosschot, Gebhardt, & Thayer, 2010).

2. Implications of left dorsolateral prefrontal cortex hyperconnectivity related to high RNT

Our observation of increased functional connectivity between bilateral STS and the left DLPFC in the high RNT group might bear significant clinical implications, as left DLPFC is a standard neuromodulation target in the treatment of resistant depression with repetitive transcranial magnetic stimulation (rTMS). rTMS has been proposed to ameliorate depressive symptoms by indirect inhibition of functional connectivity from the left DLPFC to sgACC (Baeken et al., 2014; Cole et al., 2020; Fox et al., 2014; Fox, Buckner, White, Greicius, & Pascual-Leone, 2012; George et al., 1997; George et al., 1995; Padberg & George, 2009; Tik et al., 2017). Randomized controlled trials demonstrated the antidepressant effect of high frequency (HF) rTMS and intermittent theta-burst stimulation (iTBS) applied to the left DLPFC (Avery et al., 2006; Cole et al., 2020; George et al., 2010; O'Reardon et al., 2007). Subsequently, meta-analytical evidence indicated that HF rTMS over the left DLPFC was superior to sham in the treatment of depression with a weighted mean effect size of 0.39 (95% confidence interval 0.25 to 0.54) (Cheng, Li, &

Tsai, 2021). However, the precise mechanism of action is still unknown. Another line of rTMS studies investigated the pretreatment brain imaging characteristics of depressive individuals who would respond well to rTMS since not all depressive patients effectively respond to rTMS. Similar to the connectivity changes after the treatment, several studies reported that hyperactivity in the ACC and AI predicted greater antidepressant effects of DLPFC rTMS (Baeken et al., 2014; Fox et al., 2012; Fu et al., 2021). Importantly, to the best of our knowledge, none of these studies included RNT symptoms as an individual outcome or a baseline predictive variable of DLPFC rTMS, except for one research group; they provided preliminary evidence supporting that the efficacy of DLPFC tDCS was greater in high RNT healthy individuals compared with low RNT healthy individuals (Allaert, De Raedt, van der Veen, Baeken, & Vanderhasselt, 2021; Vanderhasselt, Brunoni, Loeys, Boggio, & De Raedt, 2013). In light of our results, it might be warranted to explore whether rTMS is more effective in individuals with high RNT.

3. DMN, RNT, and depression

Following previous studies examining the relationship between RNT and the DMN, we conducted ROI-to-ROI analyses within the DMN, where we did not find significant group differences within the DMN (Supplementary Results and Figure S1). Several studies reported that RNT is associated with increased activity or connectivity within the key nodes of the DMN including the mPFC, ACC, and PCC (Apazoglou et al., 2019; Burkhouse et al., 2017; Cooney, Joormann, Eugene, Dennis, & Gotlib, 2010; Hamilton et al., 2011). Within subsystems of the DMN, several studies found increased connectivity in the anterior part of the midline core of the DMN in MDD compared to HC (Greicius et al., 2007; Li et al., 2013; Manoliu et al., 2013). Similarly, some of those studies found increased connectivity in the posterior part of the midline core of the DMN in MDD compared to HC (Li et al., 2013; Manoliu et al., 2013). On the other hand, a few studies showed decreased overall connectivity within the DMN in MDD compared to HC (Cui et al., 2021; Jacob et al., 2020; Mulders et al., 2016), which is also in line with recent two large meta-analyses showing an overall reduction within the DMN in MDD compared to HC (Tozzi et al., 2021; Yan et al., 2019). Importantly, those MDD individuals in prior studies (Jacob et al., 2020; Mulders et al., 2016; Yan et al., 2019) were mostly medicated, which could have influenced decreased DMN findings, although Tozzi and Cui only included unmedicated MDD (Cui et al., 2021; Tozzi et al., 2021).

We also conducted correlation analyses to investigate the association between connectivity within- and inter-DMN subsystems and symptom scores. We observed a marginal positive correlation between the HAMD score and connectivity within the midline core of the DMN (Figure S2.B; $r = 0.22$, p-uncorrected = 0.028, p-FDR corrected = 0.174). Our findings of slightly increased connectivity in the midline core of the DMN with a greater score of the HAMD need to be interpreted with caution since this relationship did not survive after the FDR correction.

Supplementary Tables

Table S1. Regions showing connectivity differences between high RNT and low RNT groups in the seed-to-voxel analysis.

	Hemisphere/Location	Brainnetome Atlas Label	Peak MNI coordinates	Cluster size	*t*-value
Seed1: R Anterior Superior Temporal Sulcus					
1.1	L Insular Gyrus	dId: dorsal dysgranular insular, dIa: dorsal agranular insular, vId/vIg: ventral granular insular	-36 +08 +06	597	5.49
	L Inferior Frontal Gyrus	A44v: ventral area 44, A44op: opercular area 44			
	L Precentral Gyrus	A4tl, area 4: tongue and larynx region			
	L Superior Temporal Gyrus	TE1.0 and TE1.2			
1.2	R Insular Gyrus	dId: dorsal dysgranular insular, dIa: dorsal agranular insular, vId/vIg: ventral granular insular	+42 +08 +04	455	5.65
	R Inferior Frontal Gyrus	A44v: ventral area 44, A44op: opercular area 44			
	R Precentral Gyrus	A4tl, area 4: tongue and larynx region			
	R Superior Temporal Gyrus	TE1.0 and TE1.2			
1.3	L Dorsolateral Prefrontal Cortex	A9/46d: dorsal area 9/46, A9/46v: ventral area 9/46	-34 44 22	363	5.02
1.4	L Lateral Occipital Cortex	V5/MT+: area V5/MT+	-50 -80 +12	306	-4.34
	L Angular Gyrus	A39rv: rostroventral area 39(PGa)			
1.5	L R Orbital Gyrus	A11m: medial area 11	+00 +44 -32	250	-5.84
1.6	R Angular Gyrus	A39c: caudal area 39(PGp), A39rv: rostroventral area 39(PGa)	+44 -64 +22	160	-4.23
1.7	R Parahippocampal Gyrus	A28/34: area 28/34 (EC, entorhinal cortex), A35/36c: caudal area 35/36	+18 -16 -28	130	-4.86
Seed2: L Posterior Superior Temporal Sulcus					
2.1	L R Superior Frontal Gyrus	A9l: lateral area 9, A9m,medial area 9, A10m: medial area 10	-06 +54 +34	507	-5.23
2.2	L Middle Temporal Gyrus	A21r: rostral area 21,	-46 -02 -30	333	-4.92
	L Inferior Temporal Gyrus	A20il: intermediate lateral area 20, A20iv: intermediate ventral area 20			
	L Fusiform Gyrus	A20rv: rostroventral area 20			
2.3	L Superior Temporal Sulcus	rpSTS: rostroposterior superior temporal sulcus	-44 -38 -02	202	-4.99

	L Middle Temporal Gyrus	aSTS: anterior superior temporal sulcus			
2.4	R Cerebellum Crus1/2		+24 -80 -40	154	-4.91
2.5	R Superior Temporal Sulcus	rpSTS: rostroposterior superior temporal sulcus	+52 -36 -04	148	-4.88
	R Middle Temporal Gyrus	aSTS: anterior superior temporal sulcus			
2.6	L Dorsolateral Prefrontal Cortex	A9/46v (ventral area 9/46)	-42 +46 +10	143	4.31

A voxel-wise threshold of $p < 0.001$(uncorrected) and a cluster level threshold of $p < 0.05$ (FDR-corrected) were used. RNT, repetitive negative thinking; L, left; R, right; MNI, Montreal Neurological Institute; FDR, false-discovery rate.

Table S2. Correlations between functional connectivity found in the seed-to-voxel analysis and symptom measurements.

Functional connectivity		RRS total	RRS reflection	RRS brooding	RRS depression	PHQ	OASIS
Seed1: R Superior Temporal Sulcus							
1.1	L Insular Gyrus	0.28	0.09	0.42*	0.23	-0.08	-0.20
1.2	R Insular Gyrus	0.34*	0.19	0.43*	0.28	-0.14	-0.23
1.3	L Dorsolateral Prefrontal Cortex	0.37*	0.23	0.43*	0.32	0.10	0.02
1.4	L Lateral Occipital Cortex	-0.21	-0.19	-0.31	-0.12	-0.03	-0.01
1.5	L R Orbital Gyrus	-0.35*	-0.24	-0.42*	-0.28	-0.13	0.03
1.6	R Angular Gyrus	-0.29	-0.19	-0.35*	-0.24	-0.07	-0.01
1.7	R Parahippocampal Gyrus	-0.40*	-0.27	-0.46*	-0.34*	0.02	-0.03
Seed2: L Superior Temporal Sulcus							
2.1	L R Superior Frontal Gyrus	-0.24	-0.18	-0.35*	-0.15	-0.10	-0.08
2.2	L Middle Temporal Gyrus	-0.25	-0.13	-0.33*	-0.21	-0.08	0.01
2.3	L Superior Temporal Sulcus	-0.25	-0.04	-0.42*	-0.21	-0.14	0.02
2.4	R Cerebellum Crus1/2	-0.20	-0.07	-0.34*	-0.15	-0.09	-0.14
2.5	R Superior Temporal Sulcus	-0.29	-0.14	-0.44*	-0.22	-0.10	0.13
2.6	L Dorsolateral Prefrontal Cortex	0.28	0.13	0.43*	0.21	0.21	0.05

*p<0.05 (Bonferroni-corrected) with mean head motion as a covariate. L, left; R, right; RRS, Ruminative Response Scale; PHQ, Patient Health Questionnaire-9; OASIS, Overall Anxiety Severity and Impairment Scale.

Supplementary Figures

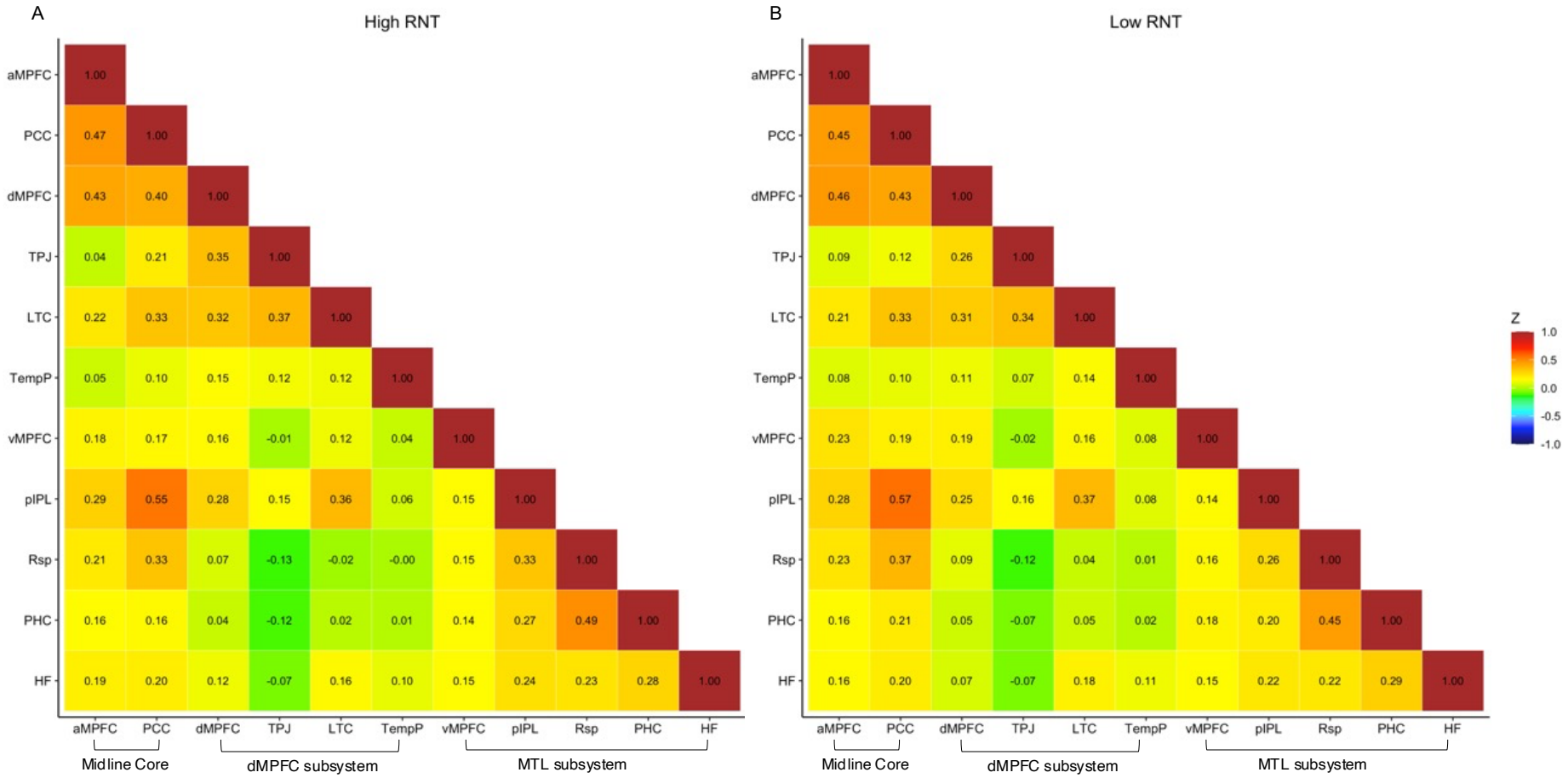

Figure S1. Average functional connectivity matrix within the DMN. A. Averaged connectivity matrices within 11 ROIs of the DMN for MDD individuals with high RNT. **B.** Averaged connectivity matrices within 11 ROIs of the DMN for MDD individuals with low RNT. The color bar indicates the Fisher's z transformed values.

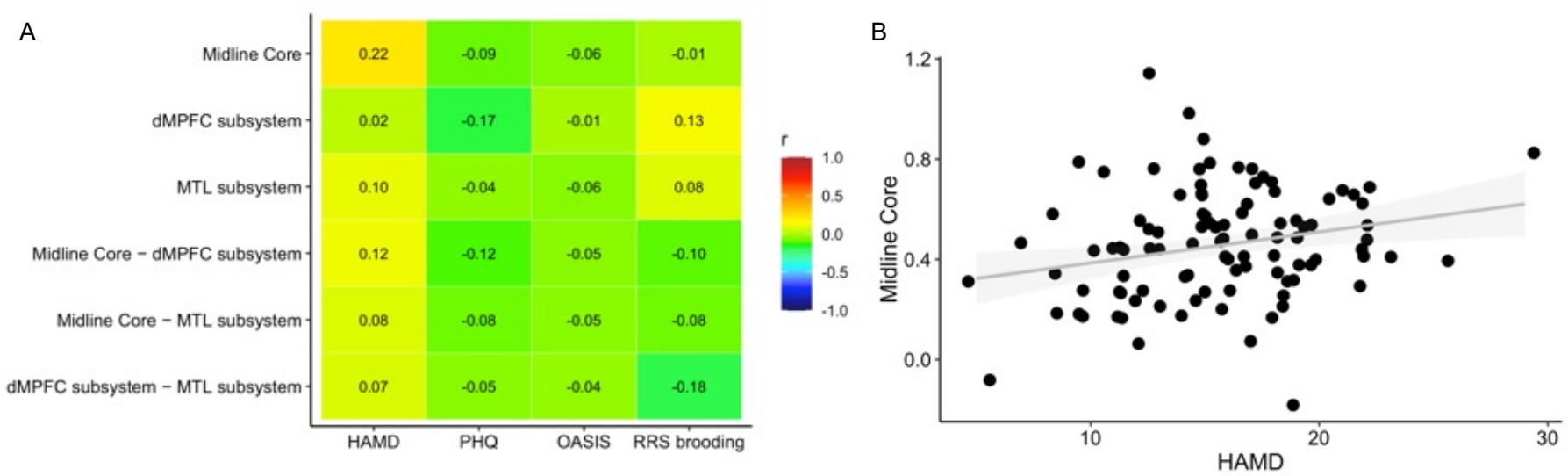

Figure S2. Association between functional connectivity within the DMN subsystems and symptom scores. A. Correlation matrices between within DMN connectivity and symptom scores. The color bar indicates Pearson's correlation coefficients. **B.** A positive correlation between functional connectivity in the midline core and HAMD (*p*-uncorrected = 0.028, *p*-FDR corrected = 0.174).

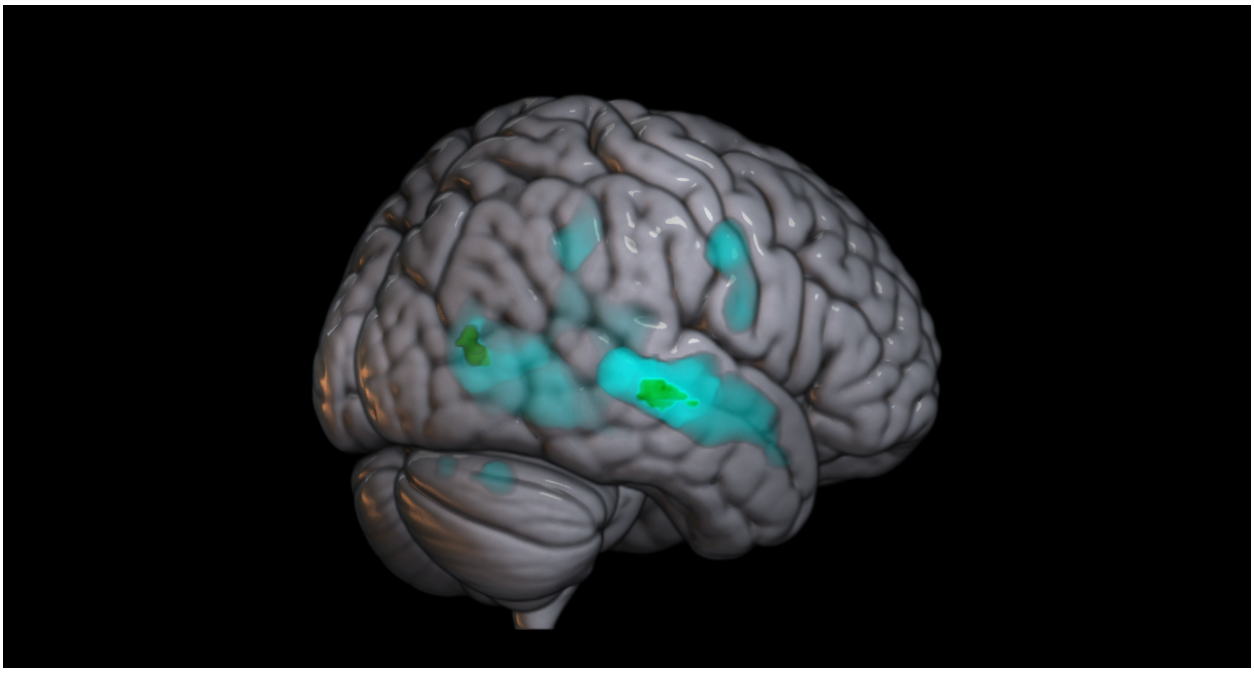

Figure S3. Clusters obtained from a whole-brain voxel-to-voxel connectivity pattern analysis and predicted neural activations related to the keywords "inner speech" in NeuroQuery. The predicted map was generated using the keywords "inner speech" (https://neuroquery.org/query?text=inner+speech) with the threshold of z-score above 3.0. The predicted map included contribution from 2192 neuroimaging studies associated with "speech" and from 695 neuroimaging studies related to "inner." The clusters obtained from voxel-to-voxel correlation analysis (rendered with green) and the downloaded predicted map from NeuroQuery (rendered with light blue) were projected to the MNI template using the MRIcroGL (https://www.nitrc.org/projects/mricrogl/).

Reference:

Allaert, J., De Raedt, R., van der Veen, F. M., Baeken, C., & Vanderhasselt, M. A. (2021). Prefrontal tDCS attenuates counterfactual thinking in female individuals prone to self-critical rumination. *Scientific Reports, 11*(1), 11601. doi:10.1038/s41598-021-90677-7

Andrews-Hanna, J. R., Reidler, J. S., Sepulcre, J., Poulin, R., & Buckner, R. L. (2010). Functional-anatomic fractionation of the brain's default network. *Neuron, 65*(4), 550-562. doi:10.1016/j.neuron.2010.02.005

Apazoglou, K., Kung, A. L., Cordera, P., Aubry, J. M., Dayer, A., Vuilleumier, P., & Piguet, C. (2019). Rumination related activity in brain networks mediating attentional switching in euthymic bipolar patients. *Int J Bipolar Disord, 7*(1), 3. doi:10.1186/s40345-018-0137-5

Avery, D. H., Holtzheimer, P. E., 3rd, Fawaz, W., Russo, J., Neumaier, J., Dunner, D. L., . . . Roy-Byrne, P. (2006). A controlled study of repetitive transcranial magnetic stimulation in medication-resistant major depression. *Biological Psychiatry, 59*(2), 187-194. doi:10.1016/j.biopsych.2005.07.003

Baeken, C., Marinazzo, D., Wu, G. R., Van Schuerbeek, P., De Mey, J., Marchetti, I., . . . De Raedt, R. (2014). Accelerated HF-rTMS in treatment-resistant unipolar depression: Insights from subgenual anterior cingulate functional connectivity. *World Journal of Biological Psychiatry, 15*(4), 286-297. doi:10.3109/15622975.2013.872295

Behzadi, Y., Restom, K., Liau, J., & Liu, T. T. (2007). A component based noise correction method (CompCor) for BOLD and perfusion based fMRI. *Neuroimage, 37*(1), 90-101. doi:10.1016/j.neuroimage.2007.04.042

Beissner, F., Meissner, K., Bar, K. J., & Napadow, V. (2013). The autonomic brain: an activation likelihood estimation meta-analysis for central processing of autonomic function. *Journal of Neuroscience, 33*(25), 10503-10511. doi:10.1523/JNEUROSCI.1103-13.2013

Burkhouse, K. L., Jacobs, R. H., Peters, A. T., Ajilore, O., Watkins, E. R., & Langenecker, S. A. (2017). Neural correlates of rumination in adolescents with remitted major depressive disorder and healthy controls. *Cognitive, Affective & Behavioral Neuroscience, 17*(2), 394-405. doi:10.3758/s13415-016-0486-4

Cheng, C. M., Li, C. T., & Tsai, S. J. (2021). Current Updates on Newer Forms of Transcranial Magnetic Stimulation in Major Depression. *Advances in Experimental Medicine and Biology, 1305*, 333-349. doi:10.1007/978-981-33-6044-0_18

Cho, J. W., Korchmaros, A., Vogelstein, J. T., Milham, M. P., & Xu, T. (2021). Impact of concatenating fMRI data on reliability for functional connectomics. *Neuroimage, 226*, 117549. doi:10.1016/j.neuroimage.2020.117549

Christoff, K., Irving, Z. C., Fox, K. C., Spreng, R. N., & Andrews-Hanna, J. R. (2016). Mind-wandering as spontaneous thought: a dynamic framework. *Nature Reviews: Neuroscience, 17*(11), 718-731. doi:10.1038/nrn.2016.113

Cole, E. J., Stimpson, K. H., Bentzley, B. S., Gulser, M., Cherian, K., Tischler, C., . . . Williams, N. R. (2020). Stanford Accelerated Intelligent Neuromodulation Therapy for Treatment-Resistant Depression. *American Journal of Psychiatry, 177*(8), 716-726. doi:10.1176/appi.ajp.2019.19070720

Cooney, R. E., Joormann, J., Eugene, F., Dennis, E. L., & Gotlib, I. H. (2010). Neural correlates of rumination in depression. *Cognitive, Affective & Behavioral Neuroscience, 10*(4), 470-478. doi:10.3758/CABN.10.4.470

Craig, A. D. (2002). How do you feel? Interoception: the sense of the physiological condition of the body. *Nature Reviews: Neuroscience, 3*(8), 655-666. doi:10.1038/nrn894
Craig, A. D. (2003). Interoception: the sense of the physiological condition of the body. *Current Opinion in Neurobiology, 13*(4), 500-505. doi:10.1016/s0959-4388(03)00090-4
Craig, A. D. (2009). How do you feel--now? The anterior insula and human awareness. *Nature Reviews: Neuroscience, 10*(1), 59-70. doi:10.1038/nrn2555
Critchley, H. D., Mathias, C. J., Josephs, O., O'Doherty, J., Zanini, S., Dewar, B. K., . . . Dolan, R. J. (2003). Human cingulate cortex and autonomic control: converging neuroimaging and clinical evidence. *Brain, 126*(Pt 10), 2139-2152. doi:10.1093/brain/awg216
Critchley, H. D., Melmed, R. N., Featherstone, E., Mathias, C. J., & Dolan, R. J. (2002). Volitional control of autonomic arousal: a functional magnetic resonance study. *Neuroimage, 16*(4), 909-919. doi:10.1006/nimg.2002.1147
Critchley, H. D., Wiens, S., Rotshtein, P., Ohman, A., & Dolan, R. J. (2004). Neural systems supporting interoceptive awareness. *Nature Neuroscience, 7*(2), 189-195. doi:10.1038/nn1176
Cui, J., Wang, Y., Liu, R., Chen, X., Zhang, Z., Feng, Y., . . . Wang, G. (2021). Effects of escitalopram therapy on resting-state functional connectivity of subsystems of the default mode network in unmedicated patients with major depressive disorder. *Transl Psychiatry, 11*(1), 634. doi:10.1038/s41398-021-01754-4
Fox, M. D., Buckner, R. L., Liu, H., Chakravarty, M. M., Lozano, A. M., & Pascual-Leone, A. (2014). Resting-state networks link invasive and noninvasive brain stimulation across diverse psychiatric and neurological diseases. *Proceedings of the National Academy of Sciences of the United States of America, 111*(41), E4367-4375. doi:10.1073/pnas.1405003111
Fox, M. D., Buckner, R. L., White, M. P., Greicius, M. D., & Pascual-Leone, A. (2012). Efficacy of transcranial magnetic stimulation targets for depression is related to intrinsic functional connectivity with the subgenual cingulate. *Biological Psychiatry, 72*(7), 595-603. doi:10.1016/j.biopsych.2012.04.028
Fu, Y., Long, Z., Luo, Q., Xu, Z., Xiang, Y., Du, W., . . . Du, L. (2021). Functional and Structural Connectivity Between the Left Dorsolateral Prefrontal Cortex and Insula Could Predict the Antidepressant Effects of Repetitive Transcranial Magnetic Stimulation. *Frontiers in Neuroscience, 15*, 645936. doi:10.3389/fnins.2021.645936
George, M. S., Lisanby, S. H., Avery, D., McDonald, W. M., Durkalski, V., Pavlicova, M., . . . Sackeim, H. A. (2010). Daily left prefrontal transcranial magnetic stimulation therapy for major depressive disorder: a sham-controlled randomized trial. *Archives of General Psychiatry, 67*(5), 507-516. doi:10.1001/archgenpsychiatry.2010.46
George, M. S., Wassermann, E. M., Kimbrell, T. A., Little, J. T., Williams, W. E., Danielson, A. L., . . . Post, R. M. (1997). Mood improvement following daily left prefrontal repetitive transcranial magnetic stimulation in patients with depression: a placebo-controlled crossover trial. *American Journal of Psychiatry, 154*(12), 1752-1756. doi:10.1176/ajp.154.12.1752
George, M. S., Wassermann, E. M., Williams, W. A., Callahan, A., Ketter, T. A., Basser, P., . . . Post, R. M. (1995). Daily repetitive transcranial magnetic stimulation (rTMS) improves mood in depression. *Neuroreport, 6*(14), 1853-1856. doi:10.1097/00001756-199510020-00008

Greicius, M. D., Flores, B. H., Menon, V., Glover, G. H., Solvason, H. B., Kenna, H., . . . Schatzberg, A. F. (2007). Resting-state functional connectivity in major depression: abnormally increased contributions from subgenual cingulate cortex and thalamus. *Biological Psychiatry, 62*(5), 429-437. doi:10.1016/j.biopsych.2006.09.020

Hamilton, J. P., Farmer, M., Fogelman, P., & Gotlib, I. H. (2015). Depressive Rumination, the Default-Mode Network, and the Dark Matter of Clinical Neuroscience. *Biological Psychiatry, 78*(4), 224-230. doi:10.1016/j.biopsych.2015.02.020

Hamilton, J. P., Furman, D. J., Chang, C., Thomason, M. E., Dennis, E., & Gotlib, I. H. (2011). Default-mode and task-positive network activity in major depressive disorder: implications for adaptive and maladaptive rumination. *Biological Psychiatry, 70*(4), 327-333. doi:10.1016/j.biopsych.2011.02.003

Jacob, Y., Morris, L. S., Huang, K. H., Schneider, M., Rutter, S., Verma, G., . . . Balchandani, P. (2020). Neural correlates of rumination in major depressive disorder: A brain network analysis. *Neuroimage Clin, 25*, 102142. doi:10.1016/j.nicl.2019.102142

Lamm, C., & Singer, T. (2010). The role of anterior insular cortex in social emotions. *Brain Structure & Function, 214*(5-6), 579-591. doi:10.1007/s00429-010-0251-3

Li, B., Liu, L., Friston, K. J., Shen, H., Wang, L., Zeng, L. L., & Hu, D. (2013). A treatment-resistant default mode subnetwork in major depression. *Biological Psychiatry, 74*(1), 48-54. doi:10.1016/j.biopsych.2012.11.007

Makovac, E., Fagioli, S., Rae, C. L., Critchley, H. D., & Ottaviani, C. (2020). Can't get it off my brain: Meta-analysis of neuroimaging studies on perseverative cognition. *Psychiatry Res Neuroimaging, 295*, 111020. doi:10.1016/j.pscychresns.2019.111020

Manoliu, A., Meng, C., Brandl, F., Doll, A., Tahmasian, M., Scherr, M., . . . Sorg, C. (2013). Insular dysfunction within the salience network is associated with severity of symptoms and aberrant inter-network connectivity in major depressive disorder. *Frontiers in Human Neuroscience, 7*, 930. doi:10.3389/fnhum.2013.00930

Menon, V. (2011). Large-scale brain networks and psychopathology: a unifying triple network model. *Trends in Cognitive Sciences, 15*(10), 483-506. doi:10.1016/j.tics.2011.08.003

Menon, V., & Uddin, L. Q. (2010). Saliency, switching, attention and control: a network model of insula function. *Brain Structure & Function, 214*(5-6), 655-667. doi:10.1007/s00429-010-0262-0

Mulders, P. C., van Eijndhoven, P. F., Pluijmen, J., Schene, A. H., Tendolkar, I., & Beckmann, C. F. (2016). Default mode network coherence in treatment-resistant major depressive disorder during electroconvulsive therapy. *Journal of Affective Disorders, 205*, 130-137. doi:10.1016/j.jad.2016.06.059

Nolen-Hoeksema, S. (2000). The role of rumination in depressive disorders and mixed anxiety/depressive symptoms. *Journal of Abnormal Psychology, 109*(3), 504-511. doi:10.1037/0021-843X.109.3.504

O'Reardon, J. P., Solvason, H. B., Janicak, P. G., Sampson, S., Isenberg, K. E., Nahas, Z., . . . Sackeim, H. A. (2007). Efficacy and safety of transcranial magnetic stimulation in the acute treatment of major depression: a multisite randomized controlled trial. *Biological Psychiatry, 62*(11), 1208-1216. doi:10.1016/j.biopsych.2007.01.018

Ottaviani, C., Thayer, J. F., Verkuil, B., Lonigro, A., Medea, B., Couyoumdjian, A., & Brosschot, J. F. (2016). Physiological concomitants of perseverative cognition: A systematic review and meta-analysis. *Psychological Bulletin, 142*(3), 231-259. doi:10.1037/bul0000036

Padberg, F., & George, M. S. (2009). Repetitive transcranial magnetic stimulation of the prefrontal cortex in depression. *Experimental Neurology, 219*(1), 2-13. doi:10.1016/j.expneurol.2009.04.020

Paulus, M. P., & Stein, M. B. (2010). Interoception in anxiety and depression. *Brain Structure & Function, 214*(5-6), 451-463. doi:10.1007/s00429-010-0258-9

Thayer, J. F., Ahs, F., Fredrikson, M., Sollers, J. J., 3rd, & Wager, T. D. (2012). A meta-analysis of heart rate variability and neuroimaging studies: implications for heart rate variability as a marker of stress and health. *Neuroscience and Biobehavioral Reviews, 36*(2), 747-756. doi:10.1016/j.neubiorev.2011.11.009

Tik, M., Hoffmann, A., Sladky, R., Tomova, L., Hummer, A., Navarro de Lara, L., . . . Windischberger, C. (2017). Towards understanding rTMS mechanism of action: Stimulation of the DLPFC causes network-specific increase in functional connectivity. *Neuroimage, 162*, 289-296. doi:10.1016/j.neuroimage.2017.09.022

Tozzi, L., Zhang, X., Chesnut, M., Holt-Gosselin, B., Ramirez, C. A., & Williams, L. M. (2021). Reduced functional connectivity of default mode network subsystems in depression: Meta-analytic evidence and relationship with trait rumination. *Neuroimage Clin, 30*, 102570. doi:10.1016/j.nicl.2021.102570

Van Dijk, K. R., Hedden, T., Venkataraman, A., Evans, K. C., Lazar, S. W., & Buckner, R. L. (2010). Intrinsic functional connectivity as a tool for human connectomics: theory, properties, and optimization. *Journal of Neurophysiology, 103*(1), 297-321. doi:10.1152/jn.00783.2009

Vanderhasselt, M. A., Brunoni, A. R., Loeys, T., Boggio, P. S., & De Raedt, R. (2013). Nosce te ipsum--Socrates revisited? Controlling momentary ruminative self-referent thoughts by neuromodulation of emotional working memory. *Neuropsychologia, 51*(13), 2581-2589. doi:10.1016/j.neuropsychologia.2013.08.011

Verkuil, B., Brosschot, J. F., Gebhardt, W. A., & Thayer, J. F. (2010). When worries make you sick: a review of perseverative cognition, the default stress response and somatic health. *Journal of Experimental Psychopathology, 1*(1), jep-009110.

Whitfield-Gabrieli, S., & Nieto-Castanon, A. (2012). Conn: a functional connectivity toolbox for correlated and anticorrelated brain networks. *Brain Connectivity, 2*(3), 125-141. doi:10.1089/brain.2012.0073

Yan, C. G., Chen, X., Li, L., Castellanos, F. X., Bai, T. J., Bo, Q. J., . . . Zang, Y. F. (2019). Reduced default mode network functional connectivity in patients with recurrent major depressive disorder. *Proceedings of the National Academy of Sciences of the United States of America, 116*(18), 9078-9083. doi:10.1073/pnas.1900390116